Eur. Phys. J. B **39**, 261–272 (2004)
DOI: 10.1140/epjb/e2004-00189-6

THE EUROPEAN PHYSICAL JOURNAL B

Dimerization in the commensurate network of 4-n-octyl-4'-cyanobiphenyl (8CB) molecules adsorbed on MoS_2 single crystal

E. Lacaze[1,a], M. Alba[2], M. Goldmann[3], J.P. Michel[1], and F. Rieutord[4]

[1] GPS, Universités Paris 6 et 7, UMR CNRS 7588, Campus Boucicaut, 140 rue de Lourmel, 75015 Paris, France
[2] LLB, UMR CEA-CNRS 12, CEA-Saclay, 91191 Gif-sur-Yvette Cedex, France
[3] LURE, bâtiment 209D, Université Paris Sud, 91405 Orsay Cedex, France
[4] CEA-Grenoble, DRFMC/SI3M/MCI, 17 rue des Martyrs, 38054 Grenoble Cedex 9, France

Received 20 December 2001 / Received in final form 1st April 2004
Published online 29 June 2004

Abstract. By combining X-ray diffraction under grazing incidence (GIXD) and scanning tunneling microscopy (STM) measurements, we have determined the structure of 4-*n*-octyl-4'-cyanobiphenyl (8CB) molecules adsorbed on MoS_2, under the thick organic film. The commensurability of the adsorbed network and the unit cell structure have been determined, revealing a complex 2D structure. This structure is characterized by straight ribbons with two types of ribbons, alternatively stacked. In one type, molecules are equally spaced, as they are paired in the other type. Considering the energetics of adsorption with a model of single ribbon, we recover the two observed ribbon structures. The alternate stacking of the ribbons appears as a consequence of the connection between the commensurabilities in the two main crystallographic directions. Moreover, we have found a particularly high value for the molecule-substrate potential corrugations, indicating that the dipole moment of 8CB molecules could play a fundamental role in the molecule-substrate interactions.

PACS. 61.10.-i X-ray diffraction and scattering – 68.35.Bs Structure of clean surfaces (reconstruction) – 61.30.-v Liquid crystals – 68.35.Md Surface thermodynamics, surface energies

1 Introduction

Studying well ordered systems leads to a deeper understanding of the relevant microscopic interactions between the objects. In this framework, the interface formed by organic molecules adsorbed on a single crystal is well adapted to the study of the interplay between different kinds of interactions. Physisorbed atoms or small molecules on crystallized surfaces can form ordered structures, commensurate or incommensurate with respect to the substrate surface. This problem has been generally studied on systems where the size of the adsorbed molecules is close to the substrate period. Theoretical models have been successfully developed and most of the observed structures and phase transitions interpreted [1]. However, if these conditions are not fulfilled (i.e. larger and/or more complex molecules) as in the case of organic molecules, the problem becomes more complicated and consequently models or simulations more or less drastically simplify the systems [2–4]. A number of techniques can be used for studying them. As an example, scanning tunneling microscopy (STM) experiments have revealed, these last fifteen years, that a number of organic molecules on metallic crystals [5–9], or on chemically inert crystals (graphite, MoS_2, etc.) [10–16], can be organized in well-ordered 2D networks. STM measurements have been used in particular to obtain models for the conformations of the adsorbed molecules, bringing informations on the respective molecule-molecule and molecule-substrate interactions [5–9,15,16]. However these informations remain usually qualitative for two main reasons. (i) STM has usually to be associated to other techniques in order to obtain quantitative informations [5]. Due to the drift phenomena of the piezoelectric materials used for scanning the sample surface, a precise determination of absolute distance values by STM is difficult to obtain. Taking into account the tip structure [17,18], it is not easy to infer the precise molecular structure from most images, since calculations are particularly heavy and the detailed nature of the tip is essentially unknown. Imaging simultaneously the substrate and the adsorbed molecules by STM, appears extremely useful in case of a semi-metal or a metal as

[a] e-mail: lacaze@gps.jussieu.fr

substrate [9,19,20] but becomes delicate in case of a semiconducting substrate. (ii) Many of the STM measurements have been performed on quite complex molecules which renders the development of quantitative models particularly difficult.

In order to go further in the understanding of these complex systems, we have chosen to study the 4-*n*-octyl-4'-cyanobiphenyl (8CB) molecules adsorbed on molybdenum disulphide (MoS_2), combining STM and X-ray diffraction under grazing incidence (GIXD). This choice was driven by the fact that although these molecules are significantly more complex than the rare gas atoms, they can be mainly described by the presence of a high dipole moment ($4.9D$) localized on the cyanobiphenyl group and a flexible alkyl chain of eight methyl groups. They consequently appear to be a good system for studying the role of the dipole moment on the molecular organization in case of physisorbed molecules.

Furthermore, preparing a thick film of 8CB on MoS_2 is rather easy and always led to reproducible STM images of the interface under such a film, whatever its thickness is (from 10 up to 1000 nm). Studying the adsorbed molecules under the thick smectic film excludes the possible use of numerous surface techniques such as Auger and LEED for example, but allows a study of the propagation of the interfacial order (8CB films being smectic at ambient temperature, this concerns the problem of anchoring in liquid crystal materials [21,22]). GIXD experiments remain possible and appear promising since STM experiments reveal a high degree of organization of the adsorbed molecules on MoS_2 [11,23] which has been interpreted as corresponding to a commensurate network [3,23]. Due to the small amount of adsorbed matter, the use of synchrotron radiations is required for the diffraction experiments. This justifies that up to now mainly STM experiments have been performed on similar physisorbed molecules. To our knowledge, organic molecules with heavy atoms incorporated, adsorbed on Ag(111), have been measured by GIXD [24,25] using a rotating anode generator and only covalently bonded alkanethiols on Au(111) [26] and 10CB molecules physisorbed on graphite have been studied by combined STM and GIXD experiments [27]. This latter system shows a metastable commensurate structure, coexisting with the a priori more stable incommensurate one. Studying such a system by GIXD is delicate since organic molecules are composed of light atoms and substrates as graphite or MoS_2 are difficult to align with respect to a synchrotron X-ray beam. However we show in this article that, combining GIXD and STM, it is possible to determine the 8CB/MoS_2 structure and so to develop a model taking into account the various microscopical intermolecular as well as molecule-substrate interactions. In the first part of this article, we describe the experimental details; the second part is devoted to the X-ray diffraction results; in a third part, we adjust the molecules position in the crystallographic cell by analyzing the peak intensities. Finally in a fourth part, we discuss the energetic balance between molecule-molecule and molecule-substrate interactions and interpret the observed adsorbed structure.

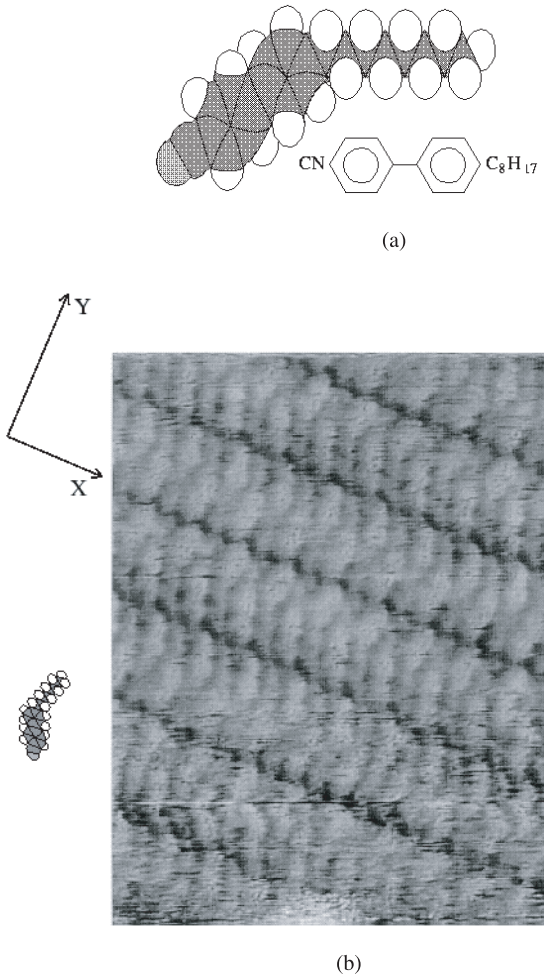

Fig. 1. (a) An enlarged view of the isolated 8CB molecule. (b) STM image of the adsorbed 8CB molecules on MoS_2 (14 nm × 14 nm; $I_t = 0.31$ nA , $V_t = 1.6$ V). The molecules on the substrate appear highly 2D ordered, organized in straight ribbons along the X-direction. Within the ribbons each molecule can be distinguished (see the model on the left), as well as within the molecules, the respective positions of the cyanobiphenyl group and the alkyl chain. From such an image it can be deduced that within the ribbons the molecules adopt an head-to-tail geometry.

2 Experimental

MoS_2 natural single crystals come from Queensland (Australia), supplied by Ward's, N.Y. This lamellar compound can be easily cleaved, revealing a clean surface parallel to the basal planes. The surface is composed of sulphur atoms organized in an hexagonal lattice (a_{MoS_2} = 3.16 Å as cell parameter), with a mosaicity smaller than 0.02°, as checked by X-ray diffraction. The 8CB (Fig. 1a) is a BDH (BDH-GMBH, Germany) product used without any further purification. The 8CB film is prepared by melting at 80 °C the organic material on top of a freshly cleaved MoS_2 substrate. An 8CB liquid crystal film, entirely covering the MoS_2 surface, is obtained with a thickness varying between 100 and 10000 Å.

In scanning tunneling microscopy (STM) experiments, the tip penetrates the non conductive bulk and probes the structure of the adsorbed molecules [10]. We systematically obtained by STM, whatever the measured area, similar images (Fig. 1b) to the ones previously published [11], indicating that, on the MoS_2 surface, under the liquid crystal film, 8CB molecules form well-organized 2D networks. It has been demonstrated on similar organic films [28] that organized mono and bilayers can be observed by STM. On the other hand, thicker crystallized films can not be measured due to their low conductivity. In the 8CB/MoS_2 system, in hundreds of experiments, terraces indicating the presence of an organized bilayer have never been observed. We have then concluded that only a single layer is 2D-crystallized under the liquid crystal film in the case of the precedently described preparation. Figure 1b reveals the high degree of 2D organization. Due to the molecules anisotropy, this organization is characterized by the formation of straight ribbons (called lamellae in some papers [12]) with a head to tail geometry of the molecules within the ribbons [11].

Grazing incidence X-ray diffraction (GIXD) experiments were performed on beam-lines BM32 at ESRF (Grenoble, France) and D41 at LURE (Orsay, France). The incident beam (photons with an 8 keV energy) reaches the interface through the 8CB bulk at an incidence of 0.3°, comparable to the MoS_2 critical angle and larger than the 8CB bulk one. The scattered intensity is scanned parallel to the surface. A vertical linear detector (PSD) ranging 13° was used at LURE-D41 where the sample was mounted horizontally, as a solid state detector was used at ESRF-BM32 where the sample was vertical. The in-plane resolution is of the order of 0.05°. The horizontal beam width is about 500 μm and its intensity is monitored. We present and analyse in this article our more complete set of measured diffraction peaks obtained on a given sample at ESRF-BM32. In this experiment, we have regularly checked the sample alignment after each reinjection and the reproducibility of our measurements, using the more intense Bragg peaks of the adsorbed structure as probe of its stability. We have observed no evolution, demonstrating a stability of the organic network within six days of beam exposure.

3 Results

30 in-plane diffraction peaks (Tab. 1, Fig. 2) of the adsorbed structure have been measured, all corresponding to $l = 0$. A close inspection of Table 1 and Figure 2 reveals that the reciprocal space associated with the measured diffraction peaks do not exactly present a 3-fold symmetry, contrary to the bare substrate case. This has to be correlated to the presence of three orientations (at ±120°) for adsorbed domains, due to the hexagonal symmetry of the MoS_2. The observation of a non 3-fold symmetry demonstrates a slightly different distribution of the diffracting domains. This distribution should be related to the sample preparation and such should essentially not spatially vary on a given sample.

Table 1. 8CB Bragg peaks integrated intensities normalized to the 2 −16 Bragg peak integrated intensity: I_m/I_o, measured intensities with the error corresponding to the adjustment between the peak and the Lorentzian curve (except for the intensities equal to 0, for which the error is estimated from the background level), I_c/I_o, calculated intensities. We obtain $R = 0.19$.

Bragg peak	I_c/I_o	I_m/I_o
0 8	0.03	0.020 ± 0.011
1 −8	0.03	0.039 ± 0.004
0 14	0	0 ± 0.014
2 −10	0	0 ± 0.013
2 0	0.69	0.76 ± 0.07
2 −16	0.94	1 ± 0.09
0 −16	0.80	0.81 ± 0.05
2 −24	0.02	0.01 ± 0.004
3 −16	0.07	0.05 ± 0.008
2 16	0.13	0.1 ± 0.02
4 −16	0.14	0.2 ± 0.03
3 8	0.02	0.01 ± 0.002
3 −32	0.04	0.03 ± 0.006
4 −24	0.03	0.06 ± 0.0004
3 −40	0.04	0.05 ± 0.006
5 0	0.01	0.02 ± 0.0007
2 32	0.40	0.31 ± 0.03
4 −48	0.44	0.67 ± 0.06
4 16	0.41	0.35 ± 0.05
6 −32	0.21	0.25 ± 0.14
6 −16	0.33	0.33 ± 0.017
0 48	0.02	0.04 ± 0.02
6 0	0.01	0 ± 0.011
6 −48	0.01	0.12 ± 0.06
−7 0	0	0 ± 0.011
2 48	0.11	0.14 ± 0.03
6 16	0.27	0.26 ± 0.06
8 −16	0.05	0.03 ± 0.008
5 40	0.02	0.01 ± 0.02
5 48	0.01	0.008 ± 0.0008

Two typical diffraction peaks are presented in Figure 3. The rocking curves are narrow, demonstrating that the adsorbed molecules structure is constituted of well-ordered single crystallized domains and confirming the high degree of 2D order of the adsorbed molecules.

The here presented diffraction peaks have all been measured at ambient temperature. In another experiment

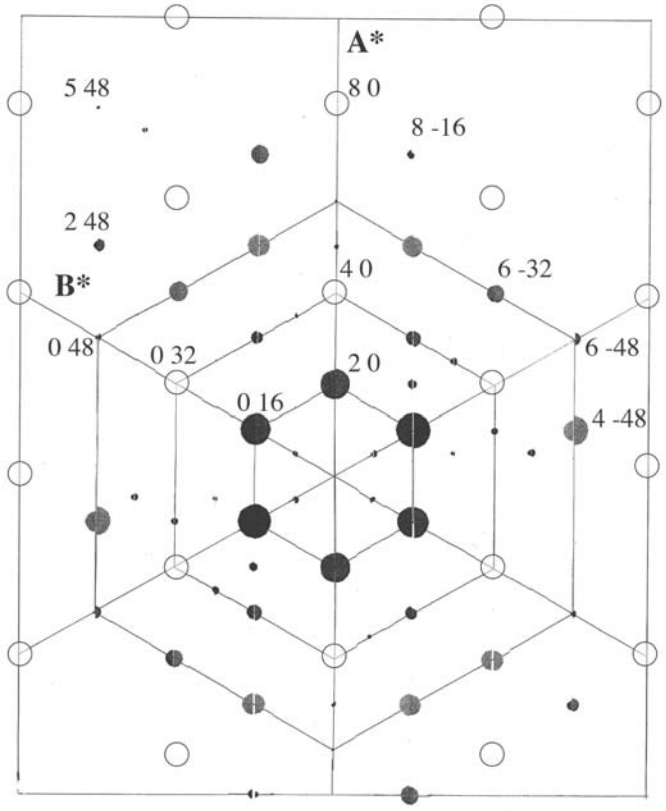

Fig. 2. Reciprocal space map of the 8CB/MoS_2 network as obtained through X-ray measurements. Compared to Table 1, the figure has been completed using the Friedel law, taking advantage of the 2D character of the 8CB/MoS_2 system which imposes equal intensities for two Bragg peaks at 180°. Open circles correspond to the MoS_2 Bragg peaks. Full circles correspond to the 8CB Bragg peaks which are indexed in the (4×32) superstructure of MoS_2. They are divided in two half circles. The areas of the right half circles are proportional to the measured intensities, whereas the areas of the left half circles are proportional to the calculated intensities.

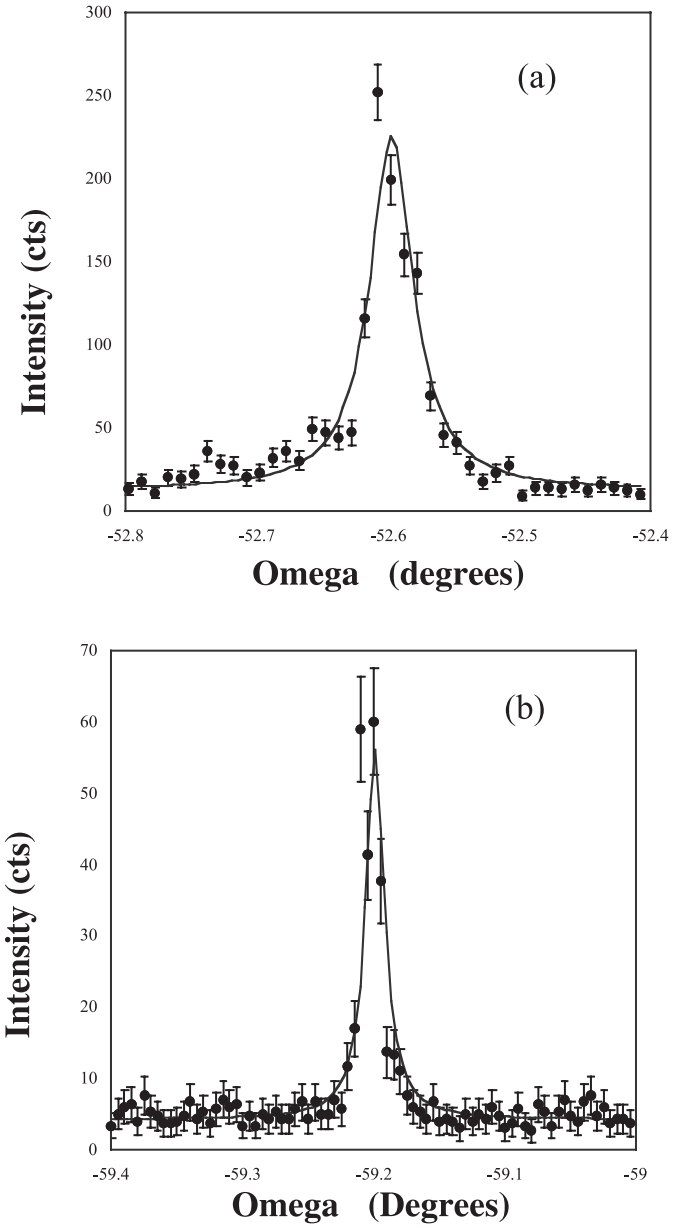

Fig. 3. (a) Rocking curve of the 2 −16 bragg peak, with the error bars corresponding to the statistical error. (b) Rocking curve of the 4 −48 bragg peak.

(ESRF-BM32) we have concentrated on the temperature evolution of some peaks intensities[1]. We did not observe any significant variation at 33 °C and 40 °C, respectively the smectic/nematic and nematic/isotropic transition temperatures of the bulk. This demonstrates that the bidimensionnal ordering of the adsorbed 8CB molecules is independent of the bulk structure and mainly related to the substrate one, which is confirmed by the observation of a commensurate structure, as discussed below.

3.1 Unit-cell size

Figure 2 presents the reciprocal lattice of the adsorbed 8CB molecules superimposed on to the MoS_2 one. This superimposition demonstrates the commensurability of the adsorbed lattice with respect to the underlying substrate one. This result confirms earlier suggestions based on STM measurements [3,23]. On a first analysis, the simplest indexing associates the molecular lattice to a (4 × 4) commensurate superstructure of the MoS_2 surface. However, such a superstructure appears inconsistent with the STM images. Indeed, it would lead to lattice parameters equal to $4 \times a_{MoS_2} = 12.5$ Å, incompatible with the width of the 8CB ribbons, estimated at about 20 Å (Fig. 1b). It is then necessary to increase one of the lattice parameter, leading to a (4 × 8) superstructure. Similarly, the STM images clearly show that two adjacent ribbons are not equivalent, but present roughly a mirror symmetry. The smallest commensurate lattice becomes then a (4 × 16)

[1] The 8CB adsorbed layer Bragg peaks start to evoluate at 120 °C, whereas the 8CB bulk already starts to evaporate around 100 °C.

superstructure. Since this lattice is aligned to the substrate one, the smaller parameter which describes the periodicity along the ribbons should be $4 \times a_{MoS_2}$ (consistent with STM measurements), corresponding to ribbons aligned to the [100] MoS_2 direction. Due to the observed commensurability of the 8CB reciprocal space with respect to the MoS_2 one (Fig. 2), the other lattice parameter can be chosen at 120° away the ribbons direction. Considering the STM images, one observes that if one molecule is translated by a unit vector $16 \times a_{MoS_2}$ an equivalent molecule is not reached. Consequently, one should add to this vector a component along the other direction. However one notices that the translation symmetry is respected if one applies twice this translation, leading to a (4×32) commensurate superstructure. For simplicity, we choose this superstructure for the observed 8CB Bragg peaks indexing (Figs. 2 and 3 and Tab. 1) leading to a crystallographic cell containing 8 molecules.

3.2 Refinement procedure

Once the commensurability is demonstrated and the 8CB crystallographic cell established, the refinement of the structure (determination of the molecules locations in the crystallographic cell) can be obtained through a fit procedure using the measured Bragg peaks integrated intensities (Tab. 1). The intensities have been obtained by a Lorentzian adjustment to the peak shapes of the rocking curves (Fig. 3). The errors indicated in Table 1 have been derivated from the adjustment. Four commensurate Bragg peaks were not observed, despite careful investigations. We have then assigned them to a null intensity in Table 1. In this case the errors have been estimated using the background level. We have finally applied the usual geometrical corrections [29] leading to the experimental values presented in Table 1.

Since the cell parameters correspond to a (4×32) MoS_2 superstructure, we started with an eight-molecule cell, built in order to form ribbons with a head to tail geometry. STM measurements suggesting that the geometry of four of these molecules (corresponding to the first two ribbons) is very close to the geometry of the four other ones (corresponding to the successive two ribbons), we divided the crystallographic cell in two identical blocks of four molecules, whose translation one from each other, along the ribbons, is considered as an adjustable parameter denoted $\delta X_{1-2-3-4/5-6-7-8}$. The molecules are assumed to lie flat on the substrate, with any distortion out of the plane of the substrate not directly taken into account. Therefore only 2D localizations have been performed. Each molecule has been divided in two rigid parts: the alkyl chain in the trans configuration and the cyanobiphenyl part also flat on the substrate. The degrees of freedom of the model are the length of the alkyl chain (L_{ALK}) and of the cyanobiphenyl group (L_{CB}) considered as equal for all molecules, the angles between these two parts (α_i) with equal values for the molecules of the same ribbon only, as suggested by STM images (Fig. 1b), the in-plane location (δX_i and δY_i) and the rotation of the molecules (β_i). A Debye-Waller term (W) has also been taken into account as well as the adsorbed network 3-fold degeneracy. Indeed, the relative weights of the three types of domains oriented at ±120° from each other must be adjusted. This gives two additional fit parameters ($Deg_{[100]}$ and $Deg_{[010]}$), the sum of the three weights being equal to 1. Note that since the commensurabilities along the two high symmetry directions of the MoS_2 substrate are multiples of each other, Bragg peaks originating from two coexisting domains can be superimposed (3-Q degeneracy). The list of all the fit parameters is presented in Table 2, with their final value, corresponding to the best adjustment between measured and calculated intensities. The starting structure for the refinement procedure (in

Table 2. Fit parameters and their calculated values: L_{CB} stands for the cyanobiphenyl length; L_{ALK} stands for the alkyl chain length; α_i stands for the angle between the cyanobiphenyl group and the alkyl chain of molecule i; β_i stands for the rotation of molecule i with respect to the direction at 120° away the ribbons; δX_i stands for the translation of molecule i, along the ribbons, with respect to molecule 1 in case of molecules 2, 3, 4, with respect to molecule 5 in case of molecules 6, 7, 8; δY_i stands for the translation of molecule i, at 120° away the ribbons, with respect to molecule 1 in case of molecules 2, 3, 4, with respect to molecule 5 in case of molecules 6, 7, 8; $\delta X_{1-2-3-4/5-6-7-8}$ stands for the translation along the ribbons between the two identical blocks (molecules (1-2-3-4) and (5-6-7-8)); W stands for the debye-waller term; $Deg_{[ij0]}$ stands for the weight of the domains oriented along the $[i\ j\ 0]$ direction with $Deg_{[100]} + Deg_{[010]} + Deg_{[-1-10]} = 1$.

Parameter description	fit value
L_{CB}	11.5 Å
L_{ALK}	11.88 Å
$\alpha_{1,2,5,6}$	40.1°
$\alpha_{3,4,7,8}$	24.3°
$\beta_{1,5}$	−16.2°
$\delta X_{2,6}$	3.29 Å
$\delta Y_{2,6}$	−0.63 Å
$\beta_{2,6}$	−10.4°
$\delta X_{3,7}$	−3.03 Å
$\delta Y_{3,7}$	23.65 Å
$\beta_{3,7}$	−11.7°
$\delta X_{4,8}$	3.59 Å
$\delta Y_{4,8}$	25.78 Å
$\beta_{4,8}$	−7.93°
$\delta X_{1-2-3-4/5-6-7-8}$	$2 \times a_{MoS_2} = 6.32$ Å
W	0.026
$Deg_{[100]}$	0.32
$Deg_{[010]}$	0.23

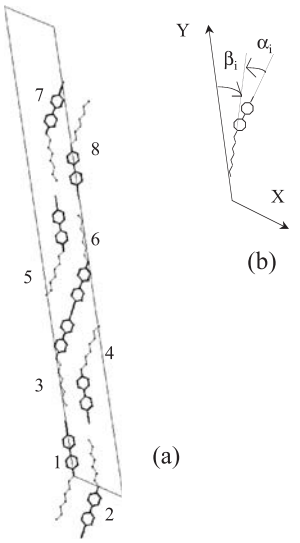

Fig. 4. (a) View of the original structure, for which $\delta X_i = \delta Y_i = 0$, $\alpha_i = 30°$ and $\beta_i = 0$. The eight molecules of the crystallographic cell are indicated. (b) Description of the refinement parameters α, the angle between the cyanobiphenyl group and the alkyl chain and β, the rotation of the molecule with respect to the direction at 120° away the ribbons (the rotation axis is located at the junction between the alkyl chain and the cyanobiphenyl group); definition of the axis X (parallel to the ribbons) and Y (at 120° away the ribbons).

which $\delta X_i = \delta Y_i = 0$, $\alpha_i = 30°$ and $\beta_i = 0$) is shown in Figure 4a, as well as the definition of α_i, β_i and the axis, X and Y, in Figure 4b. It rapidly appeared that the fit procedure do not vary some parameters ($\delta X_{1-2-3-4/5-6-7-8}$, W and α_i). These parameters have been then fixed to their final value and the accurate refinement was performed with the 14 remaining parameters. At the end of the refinement procedure, a further variation of the initially fixed parameters has been permitted without any measurable variation of their value. Despite the still large number of parameters the fit has become possible due to the strong constrains imposed by the STM images, which allow the determination of an approximate value of most of the parameters. Calculated intensities have been adjusted to the measured ones with a least square criterium and the final comparison between both is presented in Table 1.

3.3 Refinement result

The best result ($\chi^2 = 4.46$, $R = 0.19$)[2], presented in Table 2, corresponds to the crystallographic cell presented in Figure 5, a $c(4 \times 32)$ MoS_2 superstructure, and to the network shown in Figure 6. The exact parameters values presented in Table 2 are associated with uncertainties which can be roughly estimated. Regarding the uncertainty of the measured intensities, as well as the variation of the footprint between different Bragg peaks which gives an average characteristic to the weights of the three types of domains, the uncertainty is about 15 percents. Considering that the 8CB cell is eight times larger along the k-direction than along the h-direction, an STM image can be normalized in order to compensate the deformations

[2] We have also introduced anisotropic Debye-Waller terms in the refinement procedure, in order to allow different relaxations along and perpendicular to the ribbons. The obtained χ^2 is better ($\chi^2 = 3.16$, $R = 0.15$), leading to only very few variations of the other parameters, as outlined by the comparison between Table 2 and Table 3.

Table 3. Fit values when two anisotropic Debye-Waller terms are used instead of only one. $W_{H,K}$ stands for the debye-waller terms along, respectively, the H and K directions of the reciprocal space.

Parameter description	fit value
L_{CB}	11.52 Å
L_{ALK}	11.81 Å
$\alpha_{1,2,5,6}$	39.9°
$\alpha_{3,4,7,8}$	25.3°
$\beta_{1,5}$	−16.2°
$\delta X_{2,6}$	3.29 Å
$\delta Y_{2,6}$	−0.92 Å
$\beta_{2,6}$	−10.3°
$\delta X_{3,7}$	−3.05 Å
$\delta Y_{3,7}$	23.68 Å
$\beta_{3,7}$	−11.7°
$\delta X_{4,8}$	3.55 Å
$\delta Y_{4,8}$	25.7 Å
$\beta_{4,8}$	−7.42°
$\delta X_{1-2-3-4/5-6-7-8}$	$2 \times a_{MoS_2} = 6.32$ Å
W_H	0.0473
W_K	0.0
$\mathrm{Deg}_{[100]}$	0.32
$\mathrm{Deg}_{[010]}$	0.23

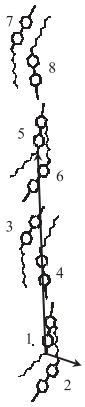

Fig. 5. View of the unit cell (plane group P1), a $c(4 \times 32)$ superstructure of MoS_2, with the eight molecules of the crystallographic cell indicated. The primitive unit cell is shown through arrows.

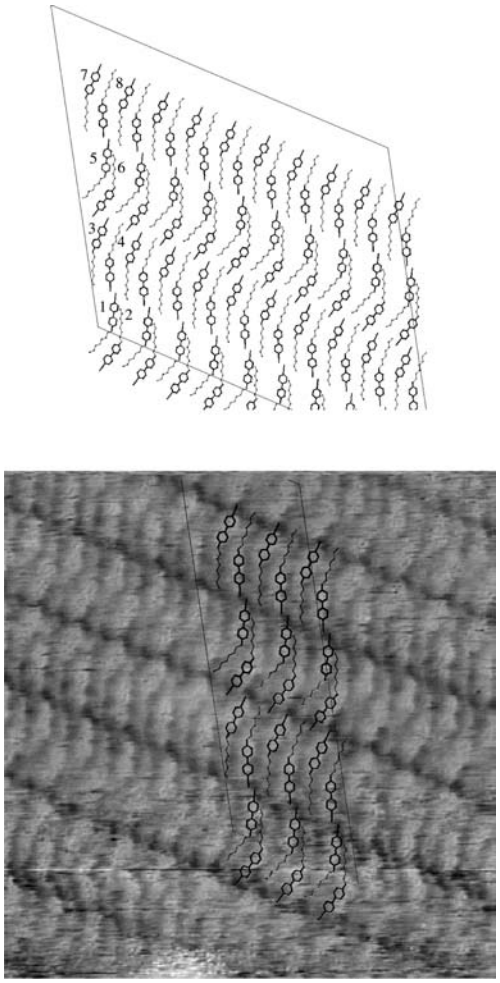

Fig. 6. (a) Result of the refinement of the X-ray data with the eight molecules of the crystallographic cell indicated. Note the formation of pairs of molecules in the ribbons associated with the molecules 1-2 and 5-6, whereas equally spaced molecules appear in the adjacent ribbons (molecules 3-4 and 7-8). (b) Comparison between the refinement and the STM image, rescaled.

induced by the drift of the piezoelectric materials and superimposed to the fit solution. Such a comparison, presented in Figure 6b, shows that the refined result is in good agreement with the STM observations, in particular the respective orientations and locations of the molecules in the cell. They can be summarized as follows.

Two ribbons (molecules 3–4 and 7–8 in Fig. 6a) are identical, with molecules equally spaced (see Fig. 6a and the value of $\delta X_{4,8} - \delta X_{3,7} = 6.62$ Å, close to $2 \times a_{MoS_2} = 6.32$ Å). In the two other ribbons (molecules 1–2 and 5–6 in Fig. 6a), also identical, the molecules are paired, demonstrating the occurrence of dimerization (see Fig. 6a and the value of $\delta X_{2,6} = 3.29$ Å). The two kinds of ribbons are alternatively stacked and the average orientation of the molecular dipoles in these two kinds of ribbons differ by an angle of roughly 10°. The non-equivalence of two successive ribbons is a particularly robust result which appears systematically in the fit solutions. Constraining an equal distance between 8CB molecules in each ribbon always leads to very large χ^2 values. Calculating, for instance, the χ^2 in case of the structure summarized in Table 2, only modified through the $\delta X_{2,6}$ term in order to impose equidistant molecules, leads to $\chi^2 = 873$. This high value is essentially associated with the 2−10 peak, which is found to be 1.23 more intense than the 2−16, as it was measured as null. Such a high intensity of the 2−10 Bragg peak systematically appears in non dimerized structures which demonstrates that the small intensity of this peak is strongly related to the appearance of dimerization in the adsorbed structure.

The obtained lengths of the alkyl chain and the cyanobiphenyl group are close (18% and 16% larger) to the ones estimated for an isolated flat molecule in a completely trans conformation. This suggests that the molecules are close to be flat on the substrate. However the obtained angles between the alkyl chain and the cyanobiphenyl group are relatively different from the one calculated for an isolated flat molecule, 35.5° (close to the one measured in a bulk crystal 34.9° [30]). This suggests in particular that the cyanobiphenyl group could be distorted with respect to a flat conformation, with possibly two different configurations for molecules of successive ribbons.

4 Discussion

4.1 Model of single ribbons

The observation of dimerization demonstrates that, although organized on a commensurate network, the adsorbed molecules lie on different adsorption sites between two successive ribbons. The origin of such a feature should be connected to the microscopic interactions between molecules as well as between molecules and substrate. In order to understand the origin of such a feature, we have built a mean-field unidimensional model associated with a single ribbon. The molecules are modelled by point dipoles, two molecules being able to be displaced in a commensurate cell of parameter $4a$ ($a_{MoS_2} = a$ for the sake of clarity), in an antiferroelectric configuration (Fig. 7). The equilibrium state is monitored by the competition between the attractive dipolar and dispersive interactions between molecules, the repulsive steric interactions between molecules and the periodic molecule-substrate interactions. Due to the knowledge of most of the physical properties of 8CB molecules, the competition can be calculated within the frame of a unidimensional model, similar to a Frenkel-Kantorowa model [31].

The intermolecular interactions are restricted to the first neighbours. In a first step, considering one neighbour only and taking r as the distance between the two molecules, the knowledge of the 8CB dipole moment ($D_{8CB} = 4.9D$ [2,32]) allows the calculation of the dipolar energy [33], $e_{Dip} = -\frac{D^2}{4\pi\epsilon_o}\frac{1}{r^3}$. Similarly, the knowledge of the 8CB polarizability ($\alpha = 40 \times 10^{-30} 4\pi\epsilon_o m^3$ [34]) and ionization potential ($I = 8$ eV is the biphenyl ionization potential, that has been increased to 8.7 eV for 8CB by

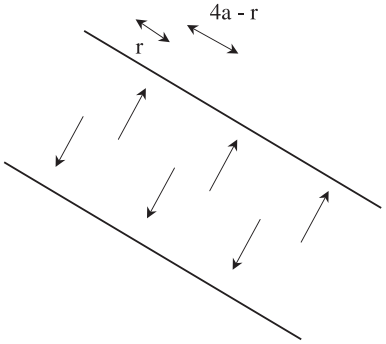

Fig. 7. Scheme of the ribbon undimensional model in which the crystallographic cell of parameter $4a$ is filled by two molecules in an antiferroelectric configuration.

analogy with the hydrocarbon case [35]) allows the calculation of the dispersive energy [33], $e_{Dis} = -\frac{3\alpha^2 I}{(4(4\pi\epsilon_o)^2)}\frac{1}{r^6}$. The attractive dispersion interactions appear to be about three to eight times larger than the attractive dipolar ones, if the distance between molecules is diminished from 6.32 to 3.29 Å, as already pointed out by Cleaver et al. [2][3]. The steric repulsion is phenomenologically accounted as usual [36]: $e_{Ste} = C\frac{1}{r^{12}}$.

In a second step we consider the two first neighbours of a given molecule, the hypothesis of commensurate cells of period $4a$ leading to intermolecular distances r and $4a-r$ (Fig. 7). In a mean-field model restricting to the interactions between first neighbours, the following energy per molecule in one ribbon, associated with the intermolecular interactions, can be calculated:

$$E = -\frac{D^2}{4\pi\epsilon_o}\left(\frac{1}{r^3} + \frac{1}{(4a-r)^3}\right) - \frac{3\alpha^2 I}{\left(4\left(4\pi\epsilon_o\right)^2\right)}\left(\frac{1}{r^6} + \frac{1}{(4a-r)^6}\right) + C\left(\frac{1}{r^{12}} + \frac{1}{(4a-r)^{12}}\right). \quad (1)$$

[3] This observation justifies the occurrence of two different structures for only slightly different molecules on the same substrate: a "single layer" one for 8CB on MoS_2, whose ribbons are characterized by an antiferroelectric alignment, a priori favorable for dipolar interactions; a "double layer" one for 10CB on MoS_2 [45], whose ribbons are characterized by a ferroelectric alignment, unfavorable for dipolar interactions [14,15]. The relative lost of dipolar energy associated with the "double layer" structure is even smaller for larger molecules (10CB compare to 8CB) and could be partly compensated by a gain in van der Waals interactions connected to the proximity of the more polarizable cyanobiphenyl groups in the second structure. So the gain in molecule-substrate interactions necessary for imposing a "double layer" structure can be only small and indeed correlated to some odd-even effect due to the position of the end of the alkyl chain on the underlying substrate, as recently proposed [14]. This remark also justifies the observation of the two types of structures evidenced on 10CB/graphite, also through the association of STM and GIXD experiments [27].

The molecule-substrate interaction has then to be added. Considering the two molecules in the cell, of positions r_A and r_B ($r = r_A - r_B$), the molecule-substrate interaction energy per molecule is

$$E_S = E_o - B/2\left(\cos 2\pi\left(\frac{r_A - R_A}{a}\right) + \cos 2\pi\left(\frac{r_B - R_B}{a}\right)\right) \quad (2)$$

R_A and R_B standing for two bottoms of substrate potential well, defined as separated by $2a$ and E_o corresponding to the adsorption energy. The value of the corrugations, B, is imposed by the interactions between substrate and molecules which include van der Waals and electrostatic interactions.

Due to the periodicity of the ribbon, the energy per molecule in one ribbon, E, can be calculated, considering the two molecules of one cell only,

$$E = E_{Dip} + E_{Dis} + E_{Ste} + E_S. \quad (3)$$

It is more convenient to choose as variable $r = r_A - r_B$, the distance between molecules A and B, and $R = (r_A + r_B)/2$, the center of mass of molecules A and B. E_S becomes

$$E_S = E_o - B\left(\cos 2\pi\left(\frac{r-2a}{2a}\right)\cos 2\pi\left(\frac{R-(R_A+R_B)/2}{a}\right)\right). \quad (4)$$

The first equilibrium condition is $\frac{\partial E}{\partial R} = 0$, leading $2\pi(\frac{R-(R_A+R_B)/2}{a}) = n\pi$, n being an integer. The cases $n \leq -2$ and $n \geq 2$ are equivalent to $n = 0$ or $n = \pm 1$, due to the periodicity a of the molecule-substrate potential.

The stability of the equilibrium imposes also $\frac{\partial^2 E}{\partial R^2} \geq 0$ which implies $\cos 2\pi(\frac{r-2a}{2a})\cos 2\pi(\frac{R-(R_A+R_B)/2}{a}) \geq 0$. If $-a/2 \leq r \leq a/2$ or $3a/2 \leq r \leq 5a/2$, $\cos 2\pi(\frac{r-2a}{2a}) \geq 0$ which induces $n = 0$, $R = (R_A + R_B)/2$. In other words, the center of mass is located in the intermediate bottom of substrate potential well defined by R_A and R_B and $E_S = E_o - B\cos 2\pi(\frac{r-2a}{2a})$. If $a/2 \leq r \leq 3a/2$, which is equivalent to $5a/2 \leq r \leq 7a/2$ due to the fact that the two distances between molecules are r and $4a-r$, the stability imposes $n = \pm 1$, $R = (R_A + R_B)/2 \pm a/2$. In other words, the center of mass is located on a top of the molecule-substrate potential and $E_S = E_o + B\cos 2\pi(\frac{r-2a}{2a})$.

In such a frame, the two types of ribbons can be analyzed as follows:

– in the first type of ribbon (molecules labelled 1–2 and 5–6 in Fig. 6a), pairing occurs which means that two distances between first neighbours can be defined, r_1 and $4a - r_1$. The intermolecular distance in an unidimensional model can be associated with the measured distance between molecules along the axis parallel to the ribbon direction and

$a/2 \leq r_1 = \delta X_{2,6} \leq 3a/2$. The center of mass is then located on a top of the molecule-substrate potential and $E_S = E_o + B\cos 2\pi(\frac{r_1-2a}{2a})$. Due to the small r_1 value, the intermolecular distance appears mainly imposed by the balance between attractive dipolar, dispersion interactions and steric repulsion;

– the second type of ribbon with equally spaced molecules (labelled 3-4 and 7-8 in Fig. 6a) corresponds to molecules located in every other bottom of substrate potential well. $r_2 = \delta X_{4,8} - \delta X_{3,7} = 6.62$ Å is indeed close to 6.32 Å. The center of mass is then located in the intermediate substrate potential well, $R = (R_A + R_B)/2$ and $E_S = E_o - B$. The intermolecular distance, r_2, is roughly two times larger than in the first type of ribbon, such that intermolecular interactions have considerably diminished. The intermolecular distance appears mainly imposed by the substrate corrugations which have to be high enough to favor such large r value which is not favorable from the point of view of intermolecular interactions.

Since the two kinds of ribbons are observed on the same sample (one ribbon with pairing adjacent to one ribbon with equally spaced molecules) one should consider a variation of the substrate corrugation parameter, B, from B_1 to B_2 between two successive ribbons. This has to be correlated to the refinement results (Tab. 2 associated with Figs. 4, 5 and 6) which indicate an average difference in the dipole orientations (the cyanobiphenyl group orientations) of about 10° between two neighboring ribbons, corresponding in particular to a higher tilt away from the direction perpendicular to the ribbons of molecules (2, 8) compare to molecules (3, 7). Such a result evidences the anisotropic nature of the molecule-substrate corrugations which depend on the orientation of the molecule with respect to the substrate crystallographic directions. It is also possible that the C amplitude of steric interactions depends on the molecules geometry, leading in particular higher C_2 (amplitude of steric interaction in ribbons with equally space molecules) than C_1 (amplitude of steric interaction in ribbons with pairing). This would avoid the possibility of intermolecular distances as small as r_1 with the molecular geometry of the second type of ribbon. This would then avoid location of molecules in every bottom of substrate potential well, leading finally to location in every other bottom of substrate potential well.

4.2 Commensurability of the ribbons

The complete 2D structure of the crystal still remains to be explained. Indeed, according to the model of a single ribbon, only the lowest energy ribbon should appear as the two type of ribbons, alternatively stacked, are observed. One can consider that the energy difference between these two kinds of ribbons is weak enough to allow the appearance of both types at room temperature. However, such consideration should lead, in a first approximation, to a statistical distribution of the two types of ribbons which is not compatible to a well ordered alternate structure. To justify such point, one needs to consider the interaction between adjacent ribbons. Calculating such energy in details appears rather complex, however one can understand the overall structure by considering qualitative arguments.

We must firstly consider that one type of ribbon is in the stable state and consequently that the adjacent one is in a higher energy state. The regular appearance of this second type of ribbon indicates that the gain in energy for the overall system is stronger that the energy difference between the two different ribbon structures.

Let's consider in a first case that the ribbons with equally spaced molecules correspond to the lower energy state. Since the molecule's locations are locked to the substrate potential, adding an identical adjacent ribbon appears strongly constraining. Indeed, considering the sterical size of the molecules, it appears that there is no possibility to keep the (4×32) superstructure and that the (4×33) is the more dense possible one. However, if the molecules in the adjacent ribbons are tilted to avoid steric incompatibilities, a dense (4×32) superstructure can be maintained. An energy loss is then associated with the molecular tilt which diminishes the substrate-molecule interactions. If the decreasing in substrate-molecule interactions is strong enough, a jump to a ribbon state with pairing can occur, favoring the intermolecular interactions, which should indeed lead to two types of ribbons, alternatively stacked. Although the ribbon energy increases for every other ribbon, the organic network density increases of about 3% with respect to the (4×33) superstructure, leading to a gain in the overall adsorption energy.

Let's now consider the other case: the ribbons with pairing correspond to the lower energy state. Adding an identical adjacent ribbon do not lead to the previous sterical problem since the molecules are tilted and not as much locked to the substrate potential. The (4×32) superstructure is then possible with only one kind of ribbon. Moreover in this type of ribbon, the inner period could be diminished, at least towards $3a$, r_2 being smaller than $3a/2$, which could allow the creation of denser ribbons, strongly suggesting that the $4a$ period is indeed imposed by the other type of ribbon.

Consequently, it appears that the stable ribbon is the one with equally spaced molecules and that the structure with pairing occurs in the way to increase the number of adsorbed 8CB molecules onto the surface. Another possibility for keeping a dense network consists in a structure with only equally spaced molecules, but whose ribbons period becomes incommensurate (for 8CB it would correspond to a superstructure between the (4×32) and the (4×33)). This can occur through deformations of the ribbons which can become kinked for example. This seems to be the case of molecules of the same series, longer than 8CB, previously studied by STM [3,37].

4.3 Molecule-substrate interaction

The comparison between energies of both types of ribbons allows now to obtain a minimum value for the substrate corrugations, which indeed stabilize the observed ribbons

with equally spaced molecules. The energy per molecule in one ribbon is

$$\begin{aligned} E \ =& -\frac{D^2}{4\pi\epsilon_o}\left(\frac{1}{r^3}+\frac{1}{(4a-r)^3}\right) \\ & -\frac{3\alpha^2 I}{(4(4\pi\epsilon_o)^2)}\left(\frac{1}{r^6}+\frac{1}{(4a-r)^6}\right) \\ & +C\left(\frac{1}{r^{12}}+\frac{1}{(4a-r)^{12}}\right) \\ & \pm B\cos 2\pi(\frac{r-2a}{2a})+E_o. \end{aligned} \tag{5}$$

Postulating that the energy of the ribbons with equally spaced molecules (E_2) is smaller than the energy of the ribbons with pairing (E_1), we can write:

$$\begin{aligned} E_2 =& -\frac{D^2}{4\pi\epsilon_o}\left(\frac{2}{r_2^3}\right)-\frac{3\alpha^2 I}{4(4\pi\epsilon_o)^2}\left(\frac{2}{r_2^6}\right) \\ & +C_2\left(\frac{2}{r_2^{12}}\right)-B_2+E_o \\ & \leq -\frac{D^2}{4\pi\epsilon_o}\left(\frac{1}{r_1^3}+\frac{1}{(4a-r_1)^3}\right) \\ & -\frac{3\alpha^2 I}{4(4\pi\epsilon_o)^2}\left(\frac{1}{r_1^6}+\frac{1}{(4a-r_1)^6}\right) \\ & +C_1\left(\frac{1}{r_1^{12}}+\frac{1}{(4a-r_1)^{12}}\right) \\ & +B_1\cos 2\pi\left(\frac{r_1-2a}{2a}\right)+E_o=E_1. \end{aligned} \tag{6}$$

Due to the different geometries of the ribbons, C_1 and C_2 can be considered as different. The term with C_2 is not taken into account, due to the high value of r_2 which renders steric interactions negligible. C_1 can be obtained through the energy minimization of the first type of ribbon:

$$\begin{aligned} C_1 =& \frac{1}{12\left(\frac{1}{r_1^{13}}-\frac{1}{(4a-r_1)^{13}}\right)}\left[\frac{3D^2}{4\pi\epsilon_o}\left(\frac{1}{r_1^4}-\frac{1}{(4a-r_1)^4}\right)\right. \\ & \left.+\frac{18\alpha^2 I}{(4(4\pi\epsilon_o)^2}\left(\frac{1}{r_1^7}-\frac{1}{(4a-r_1)^7}\right)-\frac{\pi B_1}{a}\sin 2\pi\left(\frac{r_1-2a}{2a}\right)\right] \end{aligned} \tag{7}$$

such that,

$$\begin{aligned} B_2 \geq & -\frac{D^2}{4\pi\epsilon_o}\left(\frac{2}{r_2^3}-\frac{1}{r_1^3}-\frac{1}{(4a-r_1)^3}\right. \\ & \left.+\frac{\frac{1}{r_1^{12}}+\frac{1}{(4a-r_1)^{12}}}{4\left(\frac{1}{r_1^{13}}-\frac{1}{(4a-r_1)^{13}}\right)}\left(\frac{1}{r_1^4}-\frac{1}{(4a-r_1)^4}\right)\right) \\ & -\frac{3\alpha^2 I}{(4(4\pi\epsilon_o)^2)}\left(\frac{2}{r_2^6}-\frac{1}{r_1^6}-\frac{1}{(4a-r_1)^6}\right. \\ & \left.+\frac{\frac{1}{r_1^{12}}+\frac{1}{(4a-r_1)^{12}}}{2\left(\frac{1}{r_1^{13}}-\frac{1}{(4a-r_1)^{13}}\right)}\left(\frac{1}{r_1^7}-\frac{1}{(4a-r_1)^7}\right)\right) \\ & +\frac{\pi B_1}{12a}\frac{\frac{1}{r_1^{12}}+\frac{1}{(4a-r_1)^{12}}}{\left(\frac{1}{r_1^{13}}-1(4a-r_1)^{13}\right)}\sin 2\pi\left(\frac{r_1-2a}{2a}\right) \\ & -B_1\cos 2\pi\left(\frac{r_1-2a}{2a}\right) \end{aligned} \tag{8}$$

r_1 being slightly larger than a, $\cos 2\pi(\frac{r_1-2a}{2a}) \leq 0$, $\sin 2\pi(\frac{r_1-2a}{2a})$ is close to 0 and B_2 appears finally larger than

$$\begin{aligned} B_c =& -\frac{D^2}{4\pi\epsilon_o}\left(\frac{2}{r_2^3}-\frac{1}{r_1^3}-\frac{1}{(4a-r_1)^3}\right. \\ & \left.+\frac{\frac{1}{r_1^{12}}+\frac{1}{(4a-r_1)^{12}}}{4\left(\frac{1}{r_1^{13}}-\frac{1}{(4a-r_1)^{13}}\right)}\left(\frac{1}{r_1^4}-\frac{1}{(4a-r_1)^4}\right)\right) \\ & -\frac{3\alpha^2 I}{\left(4\left(4\pi\epsilon_o\right)^2\right)}\left(\frac{2}{r_2^6}-\frac{1}{(4a-r_1)^6}\right. \\ & \left.+\frac{\frac{1}{r_1^{12}}+\frac{1}{(4a-r_1)^{12}}}{2\left(\frac{1}{r_1^{13}}-\frac{1}{(4a-r_1)^{13}}\right)}\left(\frac{1}{r_1^7}-\frac{1}{(4a-r_1)^7}\right)\right) \\ & = 6.32\times 10^{-19}\ \text{J}. \end{aligned} \tag{9}$$

The substrate corrugations which impose the presence of ribbons with equally spaced molecules appear at least

higher than 6.32×10^{-19} J, a particularly high value, of the order of $142 k_B T$, consistent with the observation of a commensurate structure at ambient temperature and with its thermal stability [note 1]. To our knowledge, no other measurement of such interactions on MoS_2 has been published. Then we have to compare our result to other systems, the best available studies dealing with graphite. In the alkane/graphite system, only van der Waals interactions exist between molecules and substrate. Changing the substrate (from graphite to MoS_2) should essentially increase the van der Waals interactions by a factor 1.5, as calculated through homogeneous models [38–42]. The substrate corrugations have been calculated through a Steele potential [43] in the case of physisorbed $C_{24}H_{50}$ alkane chains (with a number of carbon atoms similar to the 8CB, 24 with respect to 21) on graphite at about 7×10^{-21} J, 90 times smaller than our estimated value of the 8CB/MoS_2 system [44]. The 8CB/MoS_2 corrugations appear then surprisingly high.

We can postulate that B has been overestimated through our model. Calculated dipolar interactions between two 8CB molecules, exactly located in the 2D structure, increase by only 1.34 the E_D term. The van der Waals interactions between the molecules may have been overestimated due to the large distance between the more polarizable cyanobiphenyl groups in the real antiferroelectric alignment, but probably also slightly. We rather think that the 8CB/MoS_2 corrugation potential is not related to pure van der Waals interactions. The obtained strong value of the molecule-substrate corrugations could be connected to the presence of a strong dipole moment, $D_{8CB} = 4.9D$, located on the cyanobiphenyl group, through long range electrostatic interactions.

5 Conclusion

We have determined, through a combination of scanning tunneling microscopy (STM) and grazing incidence X-ray diffraction (GIXD), the 2D structure of 8CB molecules adsorbed on MoS_2, which form straight ribbons, anchored along the [100] MoS_2 direction. The structure appears to be commensurate, perpendicularly to the ribbons as predicted by a phenomenological model [3], but also within the ribbons. The 8CB crystallographic cell is a centered $c(4 \times 32)$ MoS_2 superstructure. The determination of such crystallographic parameters however is clearly not sufficient to describe correctly the adsorbed network. The intracell fine structure has also been determined by introducing constrains deduced from STM images in the refinement procedure. It demonstrates how combining these two techniques (STM and GIXD) is fruitful. In the reverse way, the X-ray results evidence the fine structures within the ribbons, which were not straightforward in the STM images.

The description of the intracell structure evidences complex intra-ribbon structures that have been interpreted through a model taking into account the microscopic interactions in a single ribbon. Two alternatively stacked types of ribbons are observed. In one type, the molecules are paired, in the other type they are equally spaced, at the bottoms of the molecule-substrate potential wells. This alternating series is probably induced by the connection between the commensurabilities along and at 120° away the ribbons, associated with the maximization of the adsorbed network density. The critical value of the molecule-substrate potential corrugations which impose the observed ribbons with equally spaced molecules has been calculated to be 6.32×10^{-19} J per molecule ($142 k_B T$). This value is particularly high (with respect to the $C_{24}H_{50}$/graphite system) and is associated with an anisotropy of the corrugations, directly connected to the orientation of the molecules with respect to the substrate crystallographic directions. Understanding these two characteristics could constitute a clue for understanding more precisely the origin of the complex molecule-substrate interactions, possibly connected to the presence of the strong 8CB dipole moment. Numerical simulations as well as similar measurements on slightly different systems could be very usefully compared to these results for such a purpose. It could allow, in the future, a direct forecast of the adsorbed molecular structures, at least in case of physisorption.

References

1. J. Villain, M. Gordon, Surf. Sci. **125**, 1 (1983)
2. D. Cleaver, D. Tildesley, Mol. Phys. **81**, 781 (1994)
3. E. Lacaze, P. Barois, R. Lacaze, J. Phys. I France **7**, 1645 (1997)
4. Y.L. Wang, W. Ji, D.X. Shi, S.X. Du, C. Seidel, Y.G. Ma, H.J. Gao, L.F. Chi, H. Fuchs, Phys. Rev. B **69**, 075408 (2004)
5. A. Soukopp, K. Glöckler, P. Kraft, S. Schmitt, M. Sokolowski, E. Umbach, Phys. Rev. B **58**, 13882 (1998)
6. M. Böhringer, K. Morgenstern, W.D. Schneider, M. Wühn, C. Wöll, R. Berndt, Surf. Sci. **444**, 199 (2000)
7. M. Schunack, E. Laegsdgaard, I. Stensgaard, F. Besenbacher, J. Chem. Phys. **117**, 8493 (2002)
8. S. Berner, M. de Wild, L. Ramoino, S. Ivan, A. Baratoff, H.J. Güntherodt, H. Suzuki, D. Schlettwein, T.A. Jung, Phys. Rev. B **68**, 115410-1 (2003)
9. P. Guaino, A.A. Cafolla, D. Carty, G. Sheerin, G. Hughes, Surf. Sci. **540**, 107 (2003)
10. J. Foster, J. Frommer, Nature **9**, 542 (1988)
11. M. Hara, Y. Iwakabe, K. Tochigi, H. Sasabe, A.F. Garito, A. Yamada, Nature **344**, 228 (1990)
12. J. Rabe, S. Buchholz, L. Askadskaya, Phys. Scripta T **49**, 200 (1993)
13. K. Walzer, M. Hietschold, J. Vac. Sci. Technol. B **14**, 1461 (1996)
14. S. Taki, T. Kadotani, S. Kai, J. Phys. Soc. Jpn **125**, 1286 (1999)
15. S. Taki, S. Kai, Jpn J. Appl. Phys. **40**, 4187 (2001)
16. N. Katsonis, A. Marchenko, D. Fichou, J. Am. Chem. Soc. **125**, 13682 (2003)
17. S. Corbel, J. Cerda, P. Sautet, Phys. Rev. B **60**, 1989 (1999)
18. F. Rosei, M. Schunack, P. Jiang, A. Gourdon, E. Laegsdgaard, I. Stensgaard, C. Joachim, F. Besenbacher, Science **296**, 328 (2002)

19. J. Poulin, H. Kagan, C. R. Acad. Sci. Paris **313**, 1533 (1991)
20. K. Walzer, M. Sternberg, M. Hietschold, Surf. Sci. **415**, 376 (1998)
21. B. Jérôme, Rep. Prog. Phys. **54**, 91 (1991)
22. E. Lacaze, J.P. Michel, M. Goldmann, M. de Boissieu, M. Gailhanou, M. Alba, Phys. Rev. E **69**, 041705 (2004)
23. D. Smith, W. Heckl, Nature **346**, 616 (1990)
24. H. Meyerheim, Th. Gloege, Phys. Stat. Sol. **173**, 175 (1999)
25. H. Meyerheim, Th. Gloege, H. Maltor, Surf. Sci. **442**, L1029 (1999)
26. T.Y.B. Leung, M.C. Gerstenberger, D.J. Lavrich, G. Scoles, F. Schreiber, G.E. Poirier, Langmuir **16**, 549 (2000)
27. P. Dai, S.-K. Wang, H. Taub, J.E. Buckley, S.N. Ehrlich, J.Z. Larese, G. Binnig, D.P.E. Smith, Phys. Rev. B **47**, 7401 (1993)
28. E. Umbach, K. Glöckler, M. Sokolowski, Surf. Sci. B **402-404**, 20 (1998)
29. D. Jacquemain, S. Grayer Wolf, F. Leveiller, M. Lahav, L. Leiserowitz, M. Deutsch, K. Kjaer, J. Als-Nielsen, J. Am. Chem. Soc. **112**, 7724 (1990)
30. M. Kuribayashi, K. Hori, Acta Cryst. C **54**, 1475 (1998)
31. J. Frenkel, T. Kantorowa, Phys. Z. SowjUn. **13**, 1 (1938); J. Frenkel, T. Kantorowa, Fis. Zh. **1**, 137 (1939)
32. K. Gueu, E. Megnassan, A. Proutierre, Mol. Cryst. Liq. Cryst. **132**, 303 (1986)
33. J. Israelachvili, *Intermolecular and surface forces* (Harcourt Brace Jovanovitch, New York, 1991)
34. M. Mitra, Phase Transitions **37**, 131 (1992)
35. F. Gutmann, L. Lyons, *Organic Semiconductors* (John Wiley and Sons, Inc., New York-London-Sidney, 1967)
36. C. Kittel, *Solid State Physics* (John Wiley and Sons, Inc., New York-Chichester-Brisbane-Toronto-Singapore, 1976)
37. Y. Iwakabe, M. Hara, K. Kondo, K. Tochigi, A. Mukoh, A. Yamada, A.F. Garito, H. Sasabe, Jpn J. Appl. Phys. Lett. **30**, 2542 (1991)
38. J. Israelachvili, Q. Rev. Biophys. **6**, 341 (1974)
39. E. Taft, H. Philipp, Phys. Rev. A **138**, 197 (1965)
40. S. Ergun, in *Chemistry and Physics of carbon*, edited by M. Dekker (P.L. Walker Jr, New York, 1968), p. 48
41. B. Evans, P. Young, Proc. Roy. Soc. A **284**, 402 (1965)
42. W. Liang, J. Phys. C **4**, L378 (1971)
43. W.A. Steele, Surf. Sci. **36**, 317 (1973)
44. R. Hentshke, B.L. Schurman, J. Rabe, J. Chem. Phys. **96**, 6213 (1992)
45. Y. Iwakabe, M. Hara, K. Kondo, S. Oh-Hara, A. Mukoh, H. Sasabe, Jpn J. Appl. Phys. Lett. **31**, L1771 (1992)